Balsa sandwich composite fracture study: Comparison of laminated to solid balsa core materials and debonding from thick balsa core materials

Meisam Shir Mohammadi and John A. Nairn*

Wood Science and Engineering, Oregon State University, Corvallis, OR 97330, USA

Abstract

We examined various fracture properties relevant to the use of balsa as a thick core material in sandwich composites with unidirectional glass fiber/vinyl ester composite skins designed for bridge decks. The first experiments compared the fracture toughness of a laminated veneer lumber (LVL) made from balsa to the toughness of conventional butcher-block balsa material. When using a good lamination adhesive, an LVL balsa core material has enhanced toughness compared to solid balsa and the LVL balsa also has enhanced fiber bridging effects. When balsa core is adhered to fiber glass composite skins, the vinyl ester resin used for bonding may infuse into the low density balsa. The second experiments looked at effects of infusing that resin on both LVL and solid balsa properties. Although the infusing caused a detrimental 15-20% increase in core material density, the infused resin had little or no affect on toughness compared to non-infused balsa. Finally, we looked at debonding toughness between fiber glass skins and a thick balsa core. The debonding toughness was higher than balsa toughness and increased with crack growth due to glass fibers bridging across the debonding fracture surface. Finite element analysis revealed that debonding a thin skin from thick balsa core in an asymmetric specimen is essentially a pure mode I process.

Keywords: A. Wood; A. Glass fibres; B. Fracture toughness; B. Debonding; C. Finite element analysis (FEA)

1. Introduction

Balsa wood is a light and fast-growing industrial hard wood that is used in many applications including thermal insulation, packaging, and sandwich composite structures [1]. In sandwich composites, balsa is a light weight core material that is used in boats, wind turbine blades, airplanes structures, and bridge decks (which is the application considered here) [1]. In such structures, balsa provides an alternative, natural material compared to other core materials such as plastic foams [2–4]. The traditional form of balsa core material has been a butcher-block structure with wood grain in the vertical or thickness direction. This form, however, was developed for convenience in delivery and fabrication and may not represent the best form of balsa as a core material. A new option for balsa wood cores is to use a wood-based composite structure known as laminated veneer lumber (LVL). LVL is a composite wood product that uses multiple layers of thin wood veneers (typically 2-3 mm thickness for each layer) with grain directions all aligned and layers bonded by adhesive. LVL balsa recently became available as a commercial product called Banova (or Baltek® VBC [5]), in which the veneers and are made by rotary peeling of balsa logs. In general, LVL made with other species is stronger, tougher, straighter, and more uniform then the corresponding solid wood (because effects of defects can be minimized by rearrangement of veneers and adhesive may contribute to properties). LVL achieves superior properties while also making up to 35% more efficient use of logs than solid lumber [6].

A concern for balsa-core sandwich composites is the development of cracks in the balsa core, which are controlled by fracture toughness properties. A previous paper [3] studied, mode I fracture parallel and perpendicular to the grain and mode II fracture parallel to the grain for solid balsa wood, which is representative of crack growth within the large blocks of butcher-block core material. Results showed that mode I toughness is reasonably high, considering balsa's low density, and that mode II fracture energy is 3-4 times higher than mode I. Nevertheless, the toughness of balsa is not high and a question arises of whether LVL balsa can provide enhanced toughness? The toughness advantages of LVL in other species can be large. Mirzaei *et al.* [7–9] compared fracture toughness of Douglas-fir (DF) and LVL of DF made with various adhesives and showed LVL has considerably higher fracture toughness than solid DF — up to four-fold increase after crack propagation. This work looked at crack propagation toughness of LVL balsa to look for enhanced toughness compared to butcher-block balsa. Because toughness enhancement in LVL is affected by adhesive [8], we looked at LVL balsa composites made using two different adhesives.

Besides the core material's fracture properties, two other fracture issues are important to sandwich composite development. First, balsa is typically bonded to fiber glass skins using vinyl ester resin. Because balsa is a low density, porous wood and vinyl ester has low viscosity, it has been observed that a significant amount of vinyl ester resin can penetrate deeply

---

*Corresponding author, john.nairn@oregonstate.edu

into the balsa core. An experimental question to answer is whether or not vinyl ester changes the fracture properties of the balsa core. To answer this equation for LVL balsa, we repeated the LVL balsa fracture experiments for specimens after infusion of bonding resins. To answer this question for solid balsa, we ran new experiments on solid balsa infused with vinyl ester resin and compared to previous experiments without infused resin [3].

The second issue is bonding of the fiber glass skin to the balsa core. Because fracture might occur at the skin/core bondline [10], it is important to consider the debonding failure mode. Several previous studies have measured skin/core debonding of balsa sandwich composites [11–15]. This paper includes new experiments to measure debonding toughness. The differences from previous work are the use of unidirectional glass fiber/vinyl ester skin layers rather that glass fabric skins and the use of thicker cores needed for bridge decks. The debonding specimen was analyzed by both analytical methods and finite element analysis to gain insight into the dominant mechanics for skin/core debonding processes in thick core composites.

2. Materials and methods

2.1. Methods

Measuring the fracture toughness of wood or of skin-core debonding can be difficult because such specimens develop process zones at the crack tip, which are characterized by wood fibers or glass fibers bridging the crack path. Such a process zone causes the fracture toughness to increase with crack propagation making it important to measure the material's R curve, which is fracture toughness as a function of crack length. The prooocess zone, however, also makes it difficult to measure crack length needed for toughness evaluation [16]. This work used an energy method to measure R, which is described elsewhere [3, 17–19]. In brief, the experiments measured force and deflection during continuous loading of double cantilever beam (DCB) specimens (see Fig. 1). The surfaces were covered with a speckle pattern that was captured in synchronized images for subsequent digital image correlation (DIC) analysis [20]. The DIC method was used to find strain in the direction normal to the crack and ahead of the crack tip. Shifts in this strain field were used to determine increments in crack growth that were added to get total crack growth. Prior work shows this method to get accurate crack lengths and to be much more accurate and objective than attempts to visually observe crack tips [3, 17, 18]. Finally, an energy analysis converted these force-deflection-crack length experiments into an energy-crack length curve. The derivative of the energy curve is the material's fracture toughness as a function of crack length or its R curve [16].

All R curves are plotted as function of crack growth defined as crack length minus the initial crack length. Due to time-consuming nature of the DIC experiments and limited availability of some specimens, the R curves were limited to results from one to five specimens. When more than
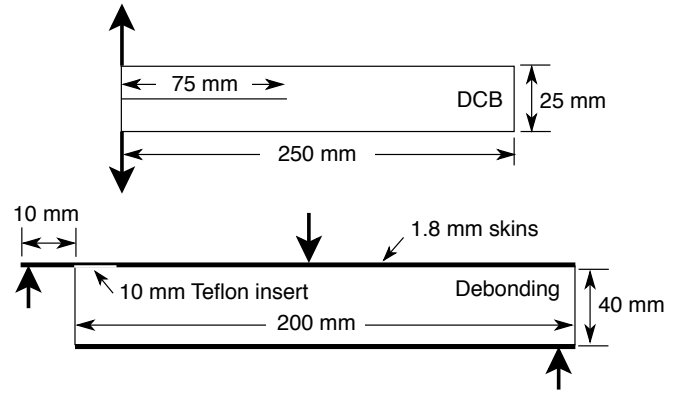
Figure 1: The top is the DCB specimen used to measure toughness in LVL balsa and solid balsa specimens. The bottom is the specimen used to measure debonding toughness. The black surfaces are the skin material. A 10 mm Teflon insert was used to create the initial crack.

one specimen was used, the R curves were averaged by dividing the curves into 10 intervals and averaging all points within each interval. Such data are plotted with error bars indicating standard deviations of points within each interval. When a single specimen was used, due to relatively few specimens available or some differences in those specimens, those R curves are reported here as curves without error bars. Despite use of a single specimen in some cases, each R curve effectively represents multiple experiments on that one specimen for toughness at each crack length. Furthermore, experience in fracture testing has shown that fracture properties are less variable than bulk strength properties because fracture is controlled by a deliberately inserted flaw while bulk properties are subject to variabilities in flaws (which can be large in wood materials).

All wood fracture experiments in this paper were TL or RL fracture, where the first letter refers to the normal to the crack plane and the second refers to the crack propagation direction. Both TL and RL propagate in the L or longitudinal direction, which means it is for crack growth parallel to the wood grain direction. The "T" and "R" refer to the crack plane normal being in the tangential and radial direction with respect to the growth rings, respectively. For LVL balsa, the use rotary cut veneers means that the "R" direction in the veneers is in the thickness direction of the veneer. In other words, RL fracture of LVL refers to a crack surface whose normal is normal to the adhesive bonds between veneers while TL fracture refers to a crack front than spans the veneer layers (see Fig. 2).

2.2. LVL Balsa

Four different types of LVL balsa samples were provided by 3A Composites for testing: G39 (non-infused and infused) and C31 (non-infused and infused). The G39 and C31 refer to the adhesive used to bond the balsa veneers when making the LVL. G39 is a polyurethane (PUR) adhesive while C31 is a urea-formaldehyde (UF) adhesive. The difference be-

2
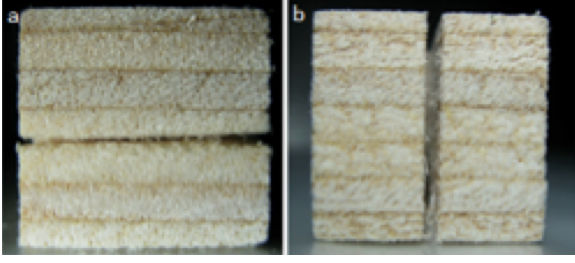
Figure 2: End view of DCB specimens used for LVL balsa toughness showing the initial saw cut for the initial crack. a. Crack cut for RL fracture. b. Crack cut for TL fracture.

tween infused and non-infused is whether or not the specimens were infused with the liquid vinyl ester resin used to bond glass/vinyl ester face sheets in the sandwich composites. The infusion was done under vacuum and the vinyl ester resin was dyed blue to help visualize resin penetration. The samples were cut to be 25×25×250 mm for mode I fracture testing in the TL and RL directions using the DCB geometry in Fig. 1. A band saw was used to cut the initial 75 mm crack.

2.3. Infused balsa

To evaluate the effect of infused resin on solid balsa as well, new fracture experiments were done on solid balsa blocks with different densities, varying from 0.2 to 0.35 g/cm^3, that were infused by liquid vinyl ester resin under vacuum. The blocks were infused and provided by 3A Composites. Each sample's density was measured after failure from material near the fracture surface. The blocks were 55×55×250 mm before impregnation and were cut to be 25×25×250 mm for mode I fracture testing in the TL and RL directions using the DCB geometry in Fig. 1. A band saw was used to cut the initial 75 mm crack. These new results were compared to baseline results for solid balsa without infused resin that were reported elsewhere [3].

2.4. Sandwich structure composites

Figure 1 shows the three-point bending specimen from Ref. [13] used to measure fracture energy for skin/core debonding in a sandwich composites. References [11, 12] used similar specimens that also loaded the skin as a single arm cantilever beam, while other skin/balsa core debonding experiments used different types of specimens [14, 15]. The skins were made from unidirectional glass fiber/vinyl-ester composites (with fiber direction in longitudinal direction of the specimens) and skin thickness of $t_1 = 1.8$ mm. The modulus of the skins along the axis of the beam was $E_1 = 46$ GPa (reported by supplier). The balsa block core had an average density 0.32 g/cm^3 and was cut such that the wood fibers were perpendicular to the skin. The thickness of the core was $t_2 = 40$ mm and modulus along the axis of the beam (which is in the transverse direction of the wood) was $E_2 = 200$ MPa (reported by supplier). The core was thicker than cores used in debonding studies on other system [11–15] because of the intended application in bridge decks. The specimens were

100 mm wide and 200 mm long. The top skin was longer, by about 10 mm, with a 10 mm pre-crack at the skin/core interface, which was made using a Teflon insert to prevent bonding. These samples were fabricated and supplied by 3A Composites. Note that these debonding specimens used butcher-block balsa core rather then the LVL balsa core because only butcher-block core specimens were available. Because experiments show a dominant failure mode to be fiber bridging of glass fibers from the skins, it is likely properties for debonding from LVL balsa cores would be similar to debonding from butcher-block balsa cores.

The experiments measured load as a function of crack length with the crack length determined by visual observation (*i.e.*, crack growth could be tracked without needing DIC methods). The fracture energy in the debonding specimen can be calculated by beam theory accounting for potential residual stresses [21]. Here the residual stresses were ignored and the beam theory result for total energy release rate, G, reduces to:

$$G = \frac{P^2 a^2}{8B}(C_\kappa^{(1)} - C_\kappa^{(3)}) \tag{1}$$

where P is load, a is crack length, B is specimen width (100 mm) and $C_\kappa^{(1)}$ and $C_\kappa^{(3)}$ are are curvature compliances for the skin and entire sandwich laminate, respectively. By simple composite beam theory, these compliances are [21]:

$$C_\kappa^{(3)} = \frac{12}{BE_1 t_1^3} \frac{S\lambda^3}{1 + 6S\lambda + 12S\lambda^2 + 8S\lambda^3}$$

$$C_\kappa^{(1)} = \frac{12}{BE_1 t_1^3} \qquad \text{and} \qquad S = \frac{E_1}{E_2} \approx 230 \tag{2}$$

where E_1 and E_2 refer to skin and balsa moduli in the beam direction and $\lambda = t_1/t_2$ is ratio of skin thickness to core thickness. This simple beam theory result ignores shear affects and cannot partition the energy into mode I and mode II components. Both its accuracy and the role of mixed mode loading were analyzed by finite element analysis (FEA). All FEA calculations were linear elastic, static, and two dimensional; they were done using the open source code NairnFEA with 8-node quadrilateral elements [22].

3. Results and discussion

3.1. LVL Balsa with G39 Adhesive

Figure 3 gives the R curves for LVL balsa with G39 adhesive in the RL (dashed lines) and TL (solid lines) directions and compares them to solid balsa (from Mohammadi and Nairn [3]) in the same directions. The LVL balsa results are for specimens both infused (as labeled) or not infused with vinyl ester resin used to bond sandwich composite skins (the rest). All LVL balsa R curves are considerably higher than the corresponding solid balsa R curves (RL *vs.* RL and TL *vs.* TL) and also increased more with crack growth indicating enhanced fiber bridging. In other words, both the toughness and the increase in toughness due to fiber bridging are higher
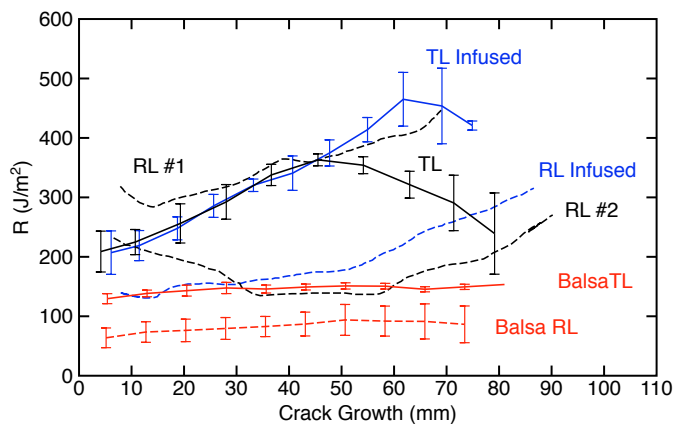
Figure 3: *R* curves for LVL balsa made with G39 adhesive in the RL and TL directions and infused on not infused with vinyl ester resin. The LVL balsa results are compared to RL and TL fracture of solid balsa (from Mohammadi and Nairn [3]).

Figure 4: *R* curves for LVL balsa made with C31 adhesive in the RL and TL directions and infused on not infused with vinyl ester resin. The LVL balsa results are compared to RL and TL fracture of solid balsa (from Mohammadi and Nairn [3]).

in LVL balsa than in solid balsa. Furthermore, while crack propagation in solid balsa often deviated from the midplane when the specimen had any grain angle misalignment [3], the crack propagation in LVL balsa remained near the midplane of the specimen. The laminated structure apparently gives more controlled specimens with well aligned grain directions. The effect of the infusing resin was minor. For RL fracture, the infused resin specimen was between two non-infused specimens. For TL fracture, the infused specimen had the same toughness at short crack length, but higher toughness at long crack length.

In the RL direction, the *R* curve for infused LVL balsa started at about 150 J/m^2 and increased to 300 J/m^2 after 90 mm of crack growth due to fiber bridging. For the non-infused RL #1 specimen, the *R* curve started at about 300 J/m^2 and increased to 450 J/m^2 after about 80 mm of crack growth. Both these specimens showed evidence of enhanced fiber-bridging effects compared to solid balsa by observation of broken fibers on the rough fracture surfaces and by more increase in *R*. The RL #2 specimen was a second non-infused specimen and was prepared differently then RL #1. For RL #1, the initial crack tip was in the middle on the central balsa veneer layer. For RL #2 , the pre-crack was cut on a glue line between two veneer layers. Although the RL #2 crack started on a glue line, it later moved into the veneer layer (*i.e.*, it did not propagate on the glue line). The *R* curve for this sample started at about 220 J/m^2, decreased to about 150 J/m^2 and then increased after reaching 60 mm or crack growth. The reason for the initial decrease in toughness may be that the notch started on a glue line, which had higher fracture energy, but soon after initiation, the crack path moved to a weaker layer (the balsa veneer in this sample). After reaching a minimum, the *R* curve the increased due to development of fiber bridging around the crack tip now within the wood layer.

In the TL direction, the infused (TL infused) and non-infused (TL) were averages of two specimens. The *R* curves
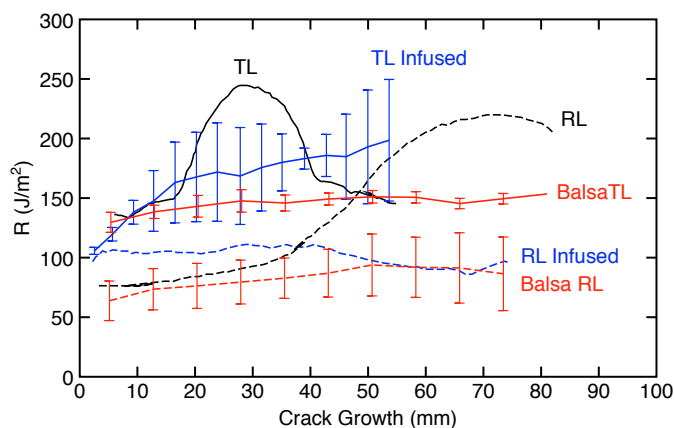
for both infused and non-infused started at about 200 J/m^2 and increased to 350 J/m^2 over the first 50 mm of crack growth. After that, the infused specimen continued to increase to 450 J/m^2 while the non-infused specimens decreased in toughness. The error bars are larger in this decreasing range because one specimen plateaued at a constant toughness of 350 J/m^2, while the other decreased to 150 J/m^2. The TL toughness is usually higher than the RL direction, likely because cracks in the TL specimen span multiple veneer glues lines while cracks in RL can be contained within a single balsa veneer layer. Compared to solid wood, the TL toughness for LVL balsa is higher and shows a larger increase in toughness due to fiber bridging.

3.2. LVL Balsa with C31 Adhesive

Figure 4 gives the *R* curves for LVL balsa with C31 adhesive in the RL (dashed lines) and TL (solid lines) directions and compares them to solid balsa (from Mohammadi and Nairn [3]) in the same directions. The LVL balsa results are for specimens both infused (as labeled) or not infused with vinyl ester resin used to bond sandwich composite skins (the rest). Unlike the G39 LVL balsa results, the *R* curves for C31 LVL balsa were much closer to the solid balsa *R* curves and therefore considerably below the G39 LVL balsa *R* curves. In the RL direction, the non-infused sample's *R* curve started from 80 J/m^2 and was identical to solid balsa for the first 40 mm of crack growth. After 40 mm of crack growth, the *R* curve increased to 210 J/m^2. The *R* curve for the RL infused specimen is very close to the solid balsa *R* curve and had mostly constant toughness (*i.e.*, no evidence of enhanced toughness due to fiber bridging).

In the TL direction, the non-infused result was a single specimen while the infused was an average of two specimens. The *R* curves for both infused and non-infused started at about 120 J/m^2 (close to solid balsa TL toughness) and increased similarly over the first 20 mm of crack growth. After that, the infused specimen continued to increase to 200 J/m^2

while the non-infused specimens had a transient increase and then, like the G39 specimens, decreased in toughness. These drops observed in a few specimens, may also be caused by sample heterogeneity and this specimen appeared to have some bond lines with insufficient adhesive. As for G39 specimens, the C31 LVL balsa R curves in TL direction were higher than in the RL direction, The C31 R curves, however, were not much different than solid balsa results and therefore much lower than G39 LVL balsa R curves.

In summary, the preferred adhesive (of the two tested) for making LVL balsa is G39 (polyurethane or PUR adhesive) because it has better fracture properties then when using C31 (urea-formaldehyde or UF adhesive). Furthermore, the G39 LVL balsa is a wood-based composite structure that has enhanced toughness and enhanced fiber bridging compared to solid balsa fracture and therefore has potential for use as an improved core material in balsa-core sandwich composites. The observation that LVL toughness can be higher than the corresponding solid wood toughness is similar to observations for other wood species [7, 8, 23]. The results here show a slight difference in balsa. With the wrong adhesive (*e.g.,* C31), very little benefit is derived from lamination, but with a good adhesive (*e.g.,* G39), the toughness can be improved. The only drawback of LVL balsa compared to solid balsa is that the adhesive used in the lamination could add weight to a core material that ideally should minimize weight. The additional weight, however, is probably minor and the material it can replace (butcher block balsa) already needs adhesive to make a sheet of core material.

The second effect studied was the effect of the vinyl ester bonding resin. The potential effects of vinyl ester depend on how it interacts with the balsa. If the resin simply fills empty lumen space in the low-density balsa, it would likely have no effect on toughness. If, however, the vinyl ester penetrates into the cell wall material, it could potentially change toughness and could be beneficial or detrimental. For LVL balsa, the results were mixed (some higher and some lower with infusion), but overall infusing resin was judged to have no significant detrimental effect on toughness.

3.3. Infused solid balsa

We measured R curves for four infused solid balsa specimens in RL fracture and four in TL fracture. The specimen densities ranged from 0.21 to 0.38 g/cm^3 prior to resin infusing and from 0.25 to 0.44 g/cm^3 after impregnation. The infusing vinyl ester resin thus caused the density to increase 15 to 20%. For individual fracture tests, we did not observe any systematic density effects or more likely, specimen-to-specimen variability effects were larger than the density effects. The results in this section therefore averaged all specimens with sufficiently straight crack propagation to get an average R curve.

The averaged R curves for infused solid balsa for RL (dashed lines) and TL (solid lines) fracture are shown in Fig. 5. The RL fracture initiated around 150 J/m^2 and had only a small increase due to fiber bridging up to about 180 J/m^2 after 90 mm of crack growth. For TL fracture the fracture again
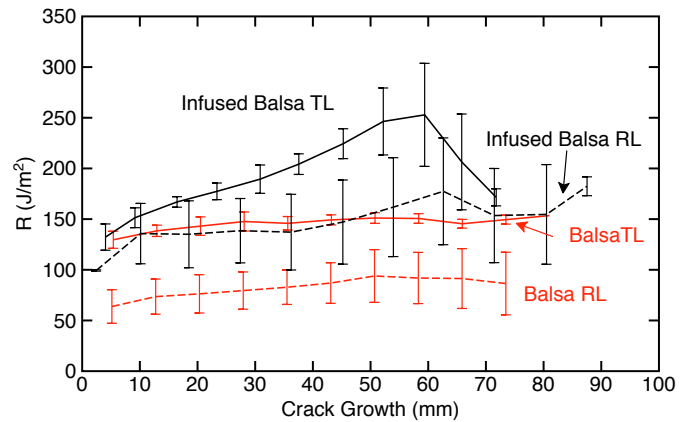
Figure 5: R curves for infused balsa in the RL and TL directions. The LVL balsa results are compared to RL and TL fracture of solid balsa (from Mohammadi and Nairn [3]).

initiated around 150 J/m^2, but it increased to 250 J/m^2 at 60 mm crack growth before a decrease at the end. As seen in all other balsa and LVL balsa fracture tests, the TL toughness is higher than RL and has larger fiber bridging effects (increase in R) due to enhanced fiber bridging.

Also included in Fig. 5 are the results for non-infused balsa from Mohammadi and Nairn [3]. The toughness for both RL and TL fracture of infused balsa were higher than the correspond solid balsa toughness. Furthermore, the solid balsa R curve showed very little increase in toughness indicating a small contribution to toughness from fiber bridging. In contrast, the infused TL specimens had in increase in toughness indicating that the vinyl ester infusion enhanced the fiber bridging contribution to toughness. This observation was qualitatively confirmed by observation that TL specimen fracture surfaces tended to be rougher than solid balsa fracture surfaces. A possible cause is non-uniformity in vinyl ester resin infusion, such that cracks may meander though weaker regions (those regions with lower resin impregnation) and fracture surfaces become rougher (raw balsa fracture surfaces were mostly flat).

In summary, resin infusion in solid balsa leads to an increase in toughness. Its only drawback on core materials would be added weight caused by the resin (*i.e.,* the 15 to 20% density increase). In other words, infusing balsa to improve toughness would come at the cost of a higher-density core material, but unavoidable infusing that occurs when bonding skins to a balsa core would not cause any degradation in the core material properties.

3.4. Skin/core debonding fracture experiments

A possible failure mode for sandwich composites is debonding between the skin and the cores, especially if the bonding has lower toughness than the core. To investigate bonding toughness in balsa core composites, we used the debonding specimen in Fig. 1 for composites with glass/vinyl ester skins to induce crack growth at the skin/core interface. For each data point (load and crack length), we first used
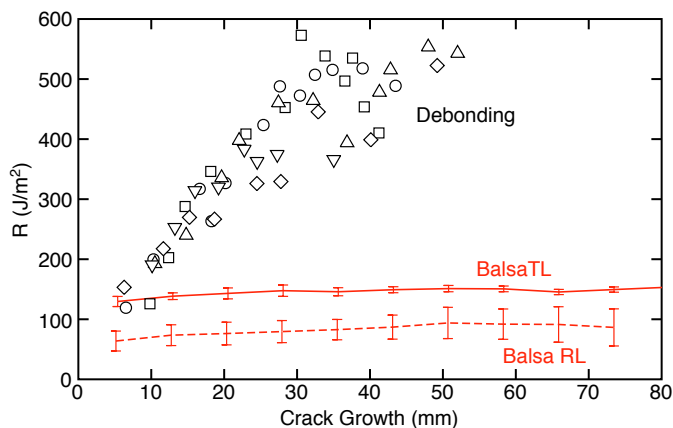
Figure 6: Debonding toughness R curve (symbols) for a unidirectional glass/vinyl ester composite bonded to a solid balsa core material. The different symbols are from five different specimens. The debonding data are compared to RL and TL fracture of solid balsa (from Mohammadi and Nairn [3]).

Figure 7: Crack process zone in a debonding specimen for glass/vinyl ester skins bonded to a solid balsa core after about 30 mm of crack growth. The black dots on the surface are positioned at 10 mm increments.

Eq. (1) to find R as a function of crack growth. The results for five different solid balsa sandwich structures are given as a scatter diagram in Fig. 6 as a function to total crack growth from the initial 10 mm Teflon insert. The debonding R curve started around 125 J/m² and increased with crack growth to 400-600 J/m². These results indicate a leveling off, or steady-state toughness of about 500 J/m². Also shown in Fig. 6 are reference curves for solid balsa. The debonding toughness is always higher than the balsa toughness and becomes significantly tougher after 30 mm of crack growth. Cantwell and Davies [11] used woven glass fibre/polyester skin, a 50 mm pre-crack, and had a thinner core material; they used $\lambda = 0.167$ while our specimens had $\lambda = 0.045$. Their results had a similar plateau behavior in the R curve and were described as having "extensive" fiber bridging [12, 13]. In comparison, however, their R curve only increased about 20% due to bridging while our results increased 300%. This difference is likely due to our unidirectional composite skins compared to their fabric composite skins and potentially due to our thicker cores. Their plateau R values where higher (around 1000 J/m²). This difference may be caused by their use of different glass/polyester/balsa materials or a thinner balsa core ($\lambda = 0.167$)

All our specimens debonded at the composite/core interface. This observation agrees with other experiments that used the same specimen [13] or a specimen that bends only the skin [11, 12]. Two other results have noted tensile failure within the balsa core away from the interface [14, 15]. These experiments, however, used a specimen that clamped the sandwich composite below the force used to pull the skin and thus loaded both the skin and the core. In other words, specimens that result in single arm bending of the skin appear better suited for measurement of debonding toughness because they are more likely to induce a pure debonding failure.

Rising R curves are associated with crack tip process zones
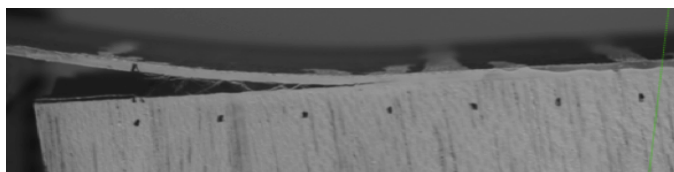
such as fiber bridging. The balsa core is oriented with the wood grain direction normal to the skin and therefore the core is unlikely to contribute to fiber bridging (unless wood fibers pull out of the end of the core). In contrast, the glass/vinyl ester skins were unidirectional composites and with sufficient bonding, fibers could pull out of the skin and bridge the crack plane gap. Figure 7 shows that the crack process zone does indicate glass fibers bridging the crack surfaces. The use of unidirectional skins is expected to enhance fiber bridging compared to similar experiments with woven glass fabric composite skins [11–13] due to greater ease of fiber pull out from the skins.

Equation (1) used for R calculations was derived using simple beam theory. It does not account for shear effects, which may be important in these specimens with fairly short aspect ratios caused by the thick core (span to depth = 200/43.6 = 4.6), and does not partition the energy into mode I and mode II components. To study these effects, we did some finite element analysis (FEA) for the debonding specimen with emphasis on effect of core thickness. To validate the FEA approach, including convergence, we began with analysis of a debonding specimen with skin thickness of $t_1 = 1$ mm, variable core thickness, t_2, and initial crack length of 40 mm. The energy release rate, including mode I and mode II components, were found by virtual crack closure methods [24]. Prior FEA calculations on bending specimens have shown that convergence works best with constant element size [24] (*e.g.*, attempts to refine the mesh around the crack tip can give unreliable results). We therefore selected element size as $s = t_1/n$ where n is the number of elements through the thickness of the skin. Provided nt_2/t_1 is an integer, the entire specimen could be meshed with equally sized elements.

Figure 8 shows convergence for mode mixity (defined as G_I/G_{tot} where G_I is mode I energy released and G_{tot} is total energy released) for test case with isotropic skin and core layers having the same moduli. The calculations were as a function of element size from one element in the skin ($s/t_1 = 1$) to four elements in the skin ($s/t_1 = 0.25$). The three results are for core to skin thicknesses of $1/\lambda = t_2/t_1 = 8$, 1, and 0, where zero means crack in the center of specimen between two skins with no core. The solid lines with open symbols are for the three-point loading configuration (see Fig. 1). For $t_2/t_1 = 8$ or 1, the mode mixity decreases as element size decreases. An extrapolation to zero element size (a quadratic fit) suggests that 3 or 4 elements in the skin provides sufficient convergence (within 0.6% of the extrapolation to zero
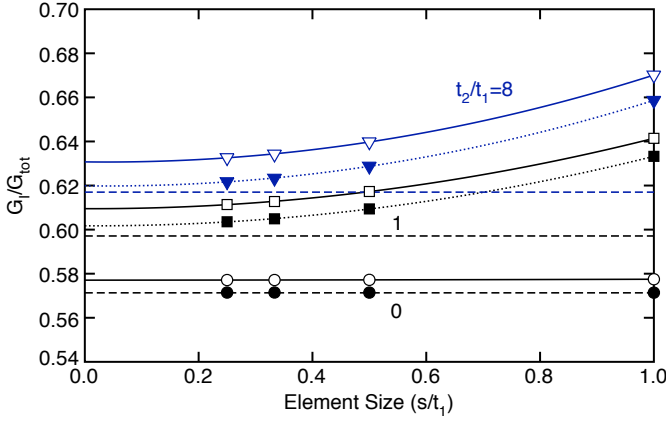
Figure 8: The mode mixity, or G_I/G_{tot}, by FEA for sandwich core composites having isotropic layers with equal moduli as a function of the constant element size and various ratios of t_2/t_1. Solid lines are for three point bending while dotted lines are for pure moment loading on the end of the skin arm. The dashed horizontal lines are theoretical results from Hutchinson and Suo [25] for pure moment loading.

element size). The specimen with no core ($t_2/t_1 = 0$) converges for all element sizes. We also looked at total energy release rate and convergence is faster. In fact any element size gives G_{tot} within 0.7% of extrapolation to zero element size; a refined mesh is only needed for finding mode mixity.

Calculations with skin and core having the same modulus were done for validation because they could be compared to a semi-analytical solution by Hutchinson and Suo [25], which considered cracks as a function of position within a beam with one arm loaded by pure bending moment. Applied to skin-core composite, they derived:

$$\frac{G_I}{G_{tot}} = \frac{K_I^2}{K_I^2 + K_{II}^2} \qquad (3)$$

where

$$K_I = \frac{M}{\sqrt{2t_1^3}}\left(\frac{(1-C_3)\sin(\omega+\gamma)}{\sqrt{V}} - \frac{C_2\cos\omega}{\sqrt{U}}\right) \qquad (4)$$

$$K_{II} = \frac{-M}{\sqrt{2t_1^3}}\left(\frac{(1-C_3)\cos(\omega+\gamma)}{\sqrt{V}} + \frac{C_2\sin\omega}{\sqrt{U}}\right) \qquad (5)$$

$$C_2 = \frac{6/\eta}{(1/\eta+1)^3}, \quad C_3 = \frac{1}{(1/\eta+1)^3}, \qquad (6)$$

$$\eta = \frac{t_1}{t_1+t_2}, \quad V = \frac{1}{12(1+\eta^3)} \qquad (7)$$

$$U = \frac{1}{1+4\eta+6\eta^2+3\eta^3} \qquad (8)$$

$$\gamma = \sin^{-1}\left(6\eta^2(1+\eta)\sqrt{UV}\right), \quad \omega = 52.1° - 3°\eta \qquad (9)$$

The last term (ω) had to be determined numerically and is claimed accurate within 1% [25]. This theoretical result for various t_2/t_1 ratios are the dashed horizontal lines and they

are 1% to 2% lower than FEA results. These discrepancies between theory and FEA were determined to be caused by boundary conditions and not by inaccuracy in either FEA or analytical methods. Although the three point bending specimen is applying a moment to the skin arm of $M = Pa/2$, where P is center point load and a is distance from support point to crack tip, this moment is not a pure bending moment. In contrast, the analytical model assumes a pure moment. We therefore modified the FEA analysis to apply pure bending by replacing the support load with a linearly varying traction from $-\sigma$ to $+\sigma$ on the end of the skin arm providing a moment resultant of $M = \sigma W t_1^2/6$, where W is specimen width. Under pure moment loading, the FEA results (dotted lines with solid symbols in Fig. 8) converge to within 0.7% of the theoretical result. Given that the numerically determined ω in Eq. (9) is only claimed to be accurate within 1%, we expect these new FEA results, which are based on more recent numerical methods, to be more accurate than the theory. In other words, these FEA results with moment loading provides confirmation that the prior theory has achieved the claimed 1% accuracy. An interesting result for the crack in the mid-plane (when $t_2/t_1 = 0$) is that simple beam theory gives both an exact total energy release rate and an exact partitioning of $G_I/G_{tot} = 4/7 = 0.571429$ [26]. Our FEA calculations agreed with this exact solution for any element size with an accuracy of better than 0.006%. This exact solution can be used to show that attempts to improve FEA efficiency by using smaller elements near the crack tip and larger elements elsewhere actually gives results that are less accurate than results using a constant element size.

The next calculations were to look at the effect of skin-to-core modulus ratio on the numerically evaluated mode mixity. Figure 9 plots mode mixity as a function of the core thickness for a variety of skin-to-core modulus ratios. As the ratio increases, the fraction mode I loading increases. For modulus ratio greater than 100 and relative core thickness greater than 8, the loading is essential pure mode I loading. For all balsa core composites, the modulus ratio was 230 and the relative core thickness was 22. Although the debonding specimen is asymmetric and intuition suggested mixed mode loading, for sandwich composites with a thick, compliant core, the test is essentially pure mode I. The R curve in Fig. 6 can therefore be considered as pure mode I debonding toughness results. Cantwell et al. [13] used FEA to look at mode mixity and also concluded the loading is predominantly mode I ($G_I/G_{tot} = 0.94$ to 0.98) and that the amount of G_I decreases as skin-to-core modulus ratio decreases. Compared to their analyses, our specimens and analyses had higher skin-to-core modulus ratio (due to unidirectional skin compared to woven fabric composite skin) and a thicker core. Both these differences led to even more predominant mode I character. Finally, Cantwell et al. [13] refined the mesh around the crack tip, which we noticed can counter-intuitively reduce accuracy compared to use of larger, constant-size elements.

Finally, to evaluate shear effects in total energy released, we did FEA calculations for each experimental data point. These calculations used actual composite three-point load-
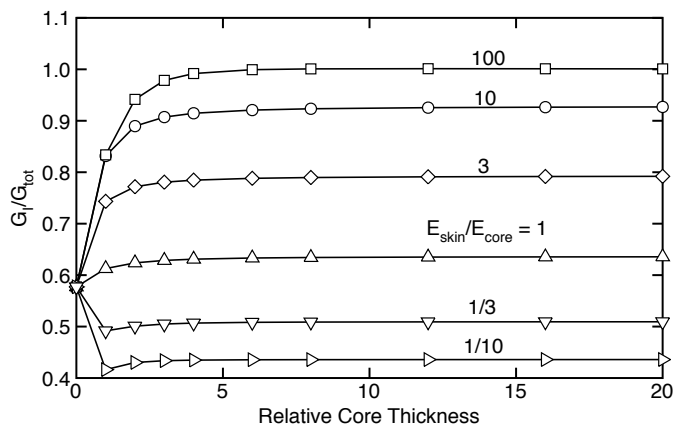
Figure 9: The mode mixity, or G_I/G_{tot}, by FEA for sandwich core composites having isotropic layers with various modulus ratios (E_1/E_2) as a function of the core thickness. The skin thickness was $t_1 = 1$ mm.
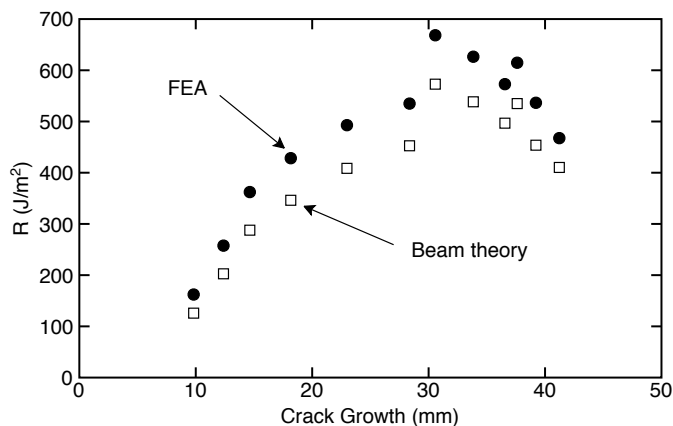
Figure 10: Total debonding toughness, R, for one specimen evaluated by beam theory in Eq. (1) (open symbols) or by FEA (solid symbols).

ing, actual dimensions ($t_1 = 1.8$ mm and $t_2 = 40$ mm), and used full anisotropic properties for the unidirectional composite skins and the solid balsa core. Because these calculations were only for total energy release rate, it was sufficient to use a single element in the skin; with nearly equally sized elements, the mesh had 22 elements in the core. Figure 10 compares R values calculated by FEA (solid symbols) to R found by beam theory using Eq. (1) for one specimen. Accounting for shear deformation caused the calculated toughness to increase 15% to 30%. The shear effect is significant in these specimens, but by both beam theory and the more-accurate FEA, the mode I debonding toughness is significantly higher than the solid core balsa toughness.

4. Conclusion

The development of sandwich composites should be accompanied by careful study of the fracture properties of the core material and of the debonding toughness between the skin and the core. A previous studied confirmed that balsa has a higher toughness compared to other low-density ma-

terials used as core materials such as foams [3]. This work extended that work to look at wood-based composite core material (LVL balsa) compared to traditional butcher-block balsa core material, potential influence of vinyl ester bonding resin infusion on core properties, and on debonding between a thick balsa core and unidirectional glass fiber composite skins. The key findings were:

- LVL balsa can potentially improve the toughness of a core material compared to solid balsa. The improvement, however, depends on adhesive used in the lamination. The polyurethane adhesive (G39) showed significant improvement, but the urea-formaldehyde adhesive (C31) showed little on no improvement.

- Infusion of vinyl ester resin into a balsa core (LVL or solid wood) did not degrade any toughness properties. The only drawback of resin infusion would be a slight increase in core density.

- The debonding toughness is higher than the core toughness and shows as large increase in R due to fiber bridging by the fibers in the unidirectional composite skin.

- Finite element analysis showed that the debonding experiments give pure mode I results whenever the skin is much stiffer than the core ($E_1/E_2 > 100$) and the core is much thicker than the skin ($t_2/t_1 > 8$).

- Compared to previous skin/core debonding studies [11–15], our results showed that both a unidirectional composite skin and a thicker core increased mode I character and that a unidirectional composite skin can enhance the increase in toughness in the R curve caused by fiber bridging. The magnitude of the plateau toughness value for our skin/bonding resin/balsa material properties differed from prior results on different materials [12, 13].

5. References

[1] K. E. Easterling, R. Harrysson, L. J. Gibson, M. F. Ashby, On the mechanics of balsa and other woods, Proc. R. Soc. Lond. A 383 (1982) 31–41.

[2] A. B. Strong, Fundamentals of composites manufacturing: materials, methods and applications, Society of Manufacturing engineers, 2008.

[3] M. S. Mohammadi, J. A. Nairn, Crack propagation and fracture toughness of solid balsa used for cores of sandwich composites, Journal of Sandwich Structures and Materials 16 (1) (2014) 22–41.

[4] N. Jover, B. Shafiq, U. Vaidya, Ballistic impact analysis of balsa core sandwich composites, Composites Part B: Engineering 67 (2014) 160 – 169.

[5] 3A Composites, BALTEK® VBC — balsa wood veneer structural core material, http://www.3accorematerials.com/baltek-vbc-balsa-veneer.html (2015).

[6] Forest Products Laboratory, Wood handbook: wood as an engineering material, General technical report FPL-GTR-190. Madison, WI: U.S. Dept. of Agriculture, Forest Service, Forest Products Laboratory, 2010.

[7] B. Mirzaei, A. Sinha, J. Nairn, Using crack propagation fracture toughness to characterize the durability of wood and wood composites, Materials & Design 87 (2015) 586 – 592.

[8] B. Mirzaei, A. Sinha, J. Nairn, Assessing the role of adhesives in durability of wood-based composites using fracture mechanics, Holzforshung 70 (8) (2016) 763–772. doi:10.1515/hf-2015-0193.

[9] B. Mirzaei, A. Sinha, J. Nairn, Measuring and modeling fiber bridging: Application to wood and wood composites exposed to moisture cycling, Composites Science and Technology 128 (2016) 65 – 74.

[10] N. Mitra, B. Raja, Improving delamination resistance capacity of sandwich composite columns with initial face/core debond, Composites Part B: Engineering 43 (3) (2012) 1604 – 1612.

[11] W. J. Cantwell, P. Davies, A test technique for assessing core-skin adhesion in composite sandwich structures, Journal of Materials Science Letters 13 (3) (1994) 203–205.

[12] W. J. Cantwell, G. Broster, P. Davies, The influence of water immersion on skin-core debonding in GFRP-balsa sandwich structures, Journal of Reinforced Plastics and Composites 15 (11) (1996) 1161–1172.

[13] W. J. Cantwell, R. Scudamore, J. Ratcliffe, P. Davies, Interfacial fracture in sandwich laminates, Comp. Sci. & Tech. 59 (1999) 2079–2085.

[14] K. N. Shivakumar, S. A. Smith, In situ fracture toughness testing of core materials in sandwich panels, Journal of Composite Materials 388 (2004) 655–668.

[15] A. Truxel, F. Avilés, L. A. Carlsson, J. L. Grenestedt, K. Millay, Influence of face/core interface on debond toughness of foam and balsa cored sandwich, Journal of Sandwich Structures and Materials 8 (3) (2006) 237–258.

[16] J. A. Nairn, Analytical and numerical modeling of r curves for cracks with bridging zones, Int. J. Fract. 155 (2009) 167–181.

[17] N. Matsumoto, J. A. Nairn, The fracture toughness of medium density fiberboard (MDF) including the effects of fiber bridging and crack-plane interference, Eng. Fract. Mech. 78 (2009) 2748–2757.

[18] N. Matsumoto, J. A. Nairn, Fracture toughness of wood and wood composites during crack propagation, Wood and Fiber Science 44 (2) (2012) 121–133.

[19] E. Wilson, J. Nairn, M. ShirMohammadi, Crack propagation fracture toughness of several wood species, Advances in Civil Engineering Materials 2 (2013) 316–327.

[20] M. A. Sutton, W. J. Wolters, W. H. Peters, W. F. Rawson, S. R. McNeil, Determination of displacement using improved digital image correlation method, Image and Vision Computing 1 (3) (1983) 133–139.

[21] J. A. Nairn, On the calculation of energy release rates for cracked laminates with residual stresses, Int. J Fract. Mech. 139 (267–293).

[22] J. A. Nairn, Material point method (NairnMPM) and finite element analysis (NairnFEA) open-source software, http://osupdocs.forestry.oregonstate.edu/index.php/Main_Page (2015).

[23] A. Sinha, J. A. Nairn, R. Gupta, The effect of elevated temperature exposure on the fracture toughness of solid wood and structural wood composites, Wood Sci. and Technol. 46 (2012) 1127–1149.

[24] J. A. Nairn, Generalized crack closure analysis for elements with arbitrarily-placed side nodes and consistent nodal forces, Int. J. Fracture 171 (2011) 11–22.

[25] J. W. Hutchinson, Z. Suo, Mixed mode cracking in layered materials, Advances in Applied Mechanics 29 (1992) 63–191.

[26] J. G. Williams, An exact result for mixed mode bending, personal communication (2014).